



CHORUS

This is the accepted manuscript made available via CHORUS. The article has been published as:

Origin of interfacial polar order in incipient ferroelectrics

Yijia Gu, Nan Wang, Fei Xue, and Long-Qing Chen

Phys. Rev. B **91**, 174103 — Published 11 May 2015

DOI: [10.1103/PhysRevB.91.174103](https://doi.org/10.1103/PhysRevB.91.174103)

Origin of Interfacial Polar Order in Incipient Ferroelectrics

Yijia Gu, Nan Wang, Fei Xue, and Long-Qing Chen

Department of Materials Science and Engineering, The Pennsylvania State University, University Park,
Pennsylvania 16802, United States

Abstract

There are ample experimental evidences indicating that the ferroelastic domain walls of incipient ferroelectrics, such as SrTiO_3 and CaTiO_3 , are polar. The emergence of such interfacial polar order at a domain wall is exciting and believed to arise from the coupling between a primary order parameter, such as strain or antiferrodistortive order parameter, and polarization. There have been several mechanisms proposed to explain the emergence of interfacial polar order, including biquadratic coupling, antiferrodistortive-antiferroelectric (AFD-AFE) coupling, and flexoelectric coupling. Using CaTiO_3 as an example, we demonstrate, using both asymptotic analytics and numerical calculation, that the flexoelectric coupling is likely the dominant mechanism leading to the interfacial polar order.

Main text

All ferroic transitions lead to the formation of domains separated by domain walls. The overall responses of a ferroic solid are often strongly influenced by the behavior of domain walls. As a matter of fact, domain walls may possess more intriguing properties than the bulk domains, for instance, high electronic conductivity¹⁻⁴, chirality^{5,6}, and oxygen vacancy segregation^{7,8} in ferroelectric domain walls and polar domain wall arising from incipient ferroelectrics⁹⁻¹⁴. It was even suggested¹⁵ that the domain walls of ferroelectrics may be treated as new engineering elements of multifunctional materials.

Domain walls have been extensively studied both experimentally^{2,10,16-23} and theoretically^{4,5,12,24-34}. In particular, the classic continuum Landau-Ginzburg-Devonshire (LGD) theory has been extensively employed to analyze both ferroelectric properties of single domains and domain walls^{35,36}. It has recently been extended to study the phenomena involving multiple order parameters at nanometer scale such as domain walls, and the results show good agreement with atomistic scale calculations^{6,37-39}. Many ferroic oxides exhibit multiple instabilities described by different soft modes or order parameters, and it is the coupling among the order parameters that yields numerous interesting phenomena such as polar domain walls in incipient ferroelectrics, incommensurate domain patterns, improper ferroelectrics, etc. To account for the interactions among order parameters, several forms of couplings have been proposed in LGD theory including biquadratic, trilinear, and flexoelectric terms. For instance, the biquadratic coupling is a

general symmetry-allowed term that describes competition between two order parameters⁵; the trilinear coupling leads to improper ferroelectrics⁴⁰; and the flexoelectric coupling produces incommensurate domain patterns⁴¹. However, the relative contributions of these coupling to the structures and properties of domain walls remain unclear. In this letter, we study the domain walls of CaTiO₃ as an example to discuss the roles of each aforementioned coupling term to the domain walls. In particular, we demonstrate that the polar domain wall in CaTiO₃ is most likely to be induced by the flexoelectric coupling.

At ambient temperature and pressure, CaTiO₃ has an orthorhombic distorted-perovskite structure with space group *Pbnm*. Disregarding the minor distortion of TiO₆ octahedra, the structure of CaTiO₃ can be illustrated as a combination of two kinds of TiO₆ octahedron tilts: two out-of-phase tilts along x_1 and x_2 directions respectively, and one in-phase tilt around x_3 direction (Glazer's notation $a^-a^-c^+$). (In this work, the coordinate system is chosen along the crystallographic directions of pseudocubic lattice.) These two kinds of tilts can also be used as order parameters to characterize the antiferrodistortive (AFD) transitions in CaTiO₃.⁴² CaTiO₃ may form several kinds of twin walls, or ferroelastic domain walls, among which the (110) twined structures, as schematically plotted in Figure 1, are the most common and intensively studied. It is shown both experimentally and theoretically that the twin wall is polar. With aberration-corrected transmission electron microscopy, the displacement pattern of Ca and Ti at the domain wall is observed which indicates nonzero polarization along x_2 direction.¹¹ A recent confocal second harmonic generation experiment also confirms the polar nature of the CaTiO₃ twin walls.¹³ Theoretical calculations showed similar predictions as well. From molecular dynamics¹⁴ and first-principles calculations¹², it is found the polarization direction is associated with the twin wall angle as indicated by the red arrows in Figure 1. In addition to the x_2 direction polarization, it is shown that there exists additional antiferroelectric (AFE)-like polarization distribution along x_1 direction by the molecular dynamics¹⁴, first-principles calculations¹² and the LGD theory⁴. Such a complicated polarization configuration inside the twin wall has been attributed to the improper AFD-AFE coupling¹², flexoelectric coupling⁴, or the biquadratic coupling⁵ by different research groups.

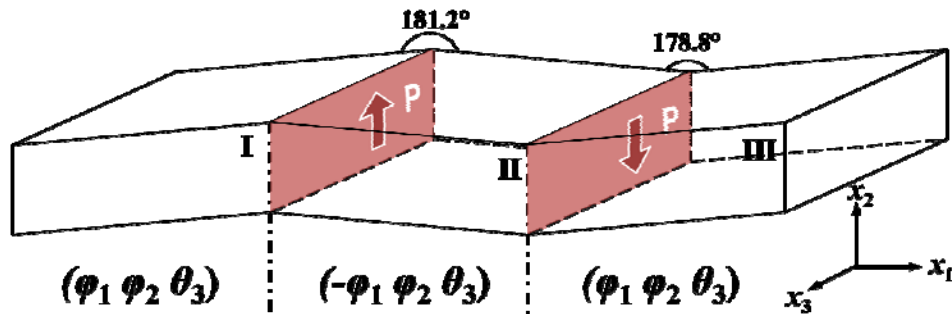


Figure 1. The schematic of the simulation system. There are three domains, I, II and III with two twin walls. The corresponding order parameters are shown for each domain. The coordinate system is chosen along crystallographic directions of the pseudocubic lattice.

In this work, we first employ the LGD theory in combination with phase-field method to elucidate the underlying thermodynamic driving forces leading to the formation of polar domain walls in CaTiO₃. We solve the state equations of LGD theory and thus get the equilibrium values of order parameters using the phase-field method⁴³. The domain structure in the phase-field model is described by the spatial distribution of order parameters (Q_i) that include spontaneous electric polarization (P_i), out-of-phase tilt (φ_i), and in-phase tilt (θ_i) in the case of CaTiO₃. The temporal evolution of the order parameters is described by time-dependent Ginzburg-Landau equations

$$\frac{\partial Q_i}{\partial t} = -L \frac{\delta F}{\delta Q_i} \quad (i = 1, 2, 3) \quad (1)$$

where L is the kinetic coefficient related to the mobility of domain walls. F is the volume integral of free energy density, which includes bulk free energy, gradient energy, elastic energy and electrostatic energy. With biquadratic coupling, the free energy density is

$$\begin{aligned} f(P_i, \varphi_i, \theta_i, \varepsilon_{ij}, E_i) = & \alpha_{ij} P_i P_j + \alpha_{ijkl} P_i P_j P_k P_l + \alpha_{ijklmn} P_i P_j P_k P_l P_m P_n - \mu_{ijkl} \varphi_i \varphi_j \theta_k \theta_l \\ & + \beta_{ij} \varphi_i \varphi_j + \beta_{ijkl} \varphi_i \varphi_j \varphi_k \varphi_l + \beta_{ijklmn} \varphi_i \varphi_j \varphi_k \varphi_l \varphi_m \varphi_n - \kappa_{ijkl} P_i P_j \theta_k \theta_l \\ & + \gamma_{ij} \theta_i \theta_j + \gamma_{ijkl} \theta_i \theta_j \theta_k \theta_l + \gamma_{ijklmn} \theta_i \theta_j \theta_k \theta_l \theta_m \theta_n - t_{ijkl} P_i P_j \varphi_k \varphi_l \\ & + \frac{1}{2} \xi_{ijkl} \left(\frac{\partial P_i}{\partial x_j} \frac{\partial P_k}{\partial x_l} \right) + \frac{1}{2} v_{ijkl} \left(\frac{\partial \varphi_i}{\partial x_j} \frac{\partial \varphi_k}{\partial x_l} \right) + \frac{1}{2} \omega_{ijkl} \left(\frac{\partial \theta_i}{\partial x_j} \frac{\partial \theta_k}{\partial x_l} \right) \\ & + \frac{1}{2} s_{ijkl} \sigma_{ij} \sigma_{kl} - Q_{ijkl} \sigma_{ij} P_k P_l - R_{ijkl} \sigma_{ij} \varphi_k \varphi_l - G_{ijkl} \sigma_{ij} \theta_k \theta_l \\ & - P_i E_j - \frac{1}{2} \varepsilon_0 \kappa_{ij}^b E_i E_j \end{aligned} \quad (2)$$

where α , β , and γ are Landau-Devonshire coefficients (only the coefficients of the second order terms are temperature dependent), ξ_{ijkl} , v_{ijkl} and ω_{ijkl} are the anisotropic gradient energy coefficients of polarization, out-of-phase tilt and in-phase tilt respectively, t_{ijkl} , κ_{ijkl} , g_{ijkl} , μ_{ijkl} , λ_{ijkl} , and ς_{ijkl} are coupling coefficients, s_{ijkl} is the elastic compliance tensor, σ_{ij} is the stress, E_i is the external electric field, ε_0 is the dielectric permittivity of vacuum, and κ_{ij}^b is the background dielectric constant. All the coefficients can be found in Ref⁴².

Phase-field simulation using the free energy expression (2) is performed to examine the effect of biquadratic coupling between the structural order parameters (φ and θ) and its possible role in the generation of polar domain walls. The simulation system setup also follows Figure 1. It includes three domains and two domain walls. The domain walls lie in the x_2 - x_3 plane and perpendicular to the x_1 direction. To compare with the existing results of CaTiO_3 domain walls, we choose the same twin structure as in previous works^{11,12,14}. The order parameters in domain I, II and III are therefore $(\varphi_1, \varphi_2, \theta_3)$, $(-\varphi_1, \varphi_2, \theta_3)$ and $(\varphi_1, \varphi_2, \theta_3)$, respectively. The system is then simplified to a one-dimensional problem with the simulation size $4096\Delta x \times 1\Delta x \times 1\Delta x$ using the three-dimensional phase-field model. The grid size Δx is chosen to be 0.25 nm. Periodical boundary condition is imposed along each direction. The stress field is calculated using Kachaturyan's microelastic theory⁴⁴, and the electric depolarization field is obtained by solving Poisson's equation⁴⁵. To get the designed twin structures, we start our simulation with the preassigned order parameter values ($P_1 = P_2 = 0.1 \text{ C/m}^2$, and $\varphi_1 = \varphi_2 = -\theta_3 = -5 \text{ pm}$), and then let the system relax to equilibrium. The calculated equilibrium values for the structural order parameters are 5.64 pm and 5.89 pm for out-of-phase tilt components and in-phase tilt component, respectively. These values agree well with literature^{12,46,47}. The calculated angle between the two domains is 178.8° , which is identical to experimental observations¹¹. However, no polarization is observed at the domain wall and throughout the whole simulation system.

Since the phase-field numerics above may be sensitive to the coefficients of the free energy, a generalized near-interface asymptotic analysis⁴⁸ of the phase-field model with biquadratic coupling is also carried out here to support our conclusion. First, to simplify analytics, electrostatic contribution is ignored. The total free energy with up to fourth order terms is then

$$\begin{aligned}
f^B(P_1, P_2, \varphi_1, \varphi_2, \theta_3) = & \alpha_1(P_1^2 + P_2^2) + \alpha_{11}(P_1^2 + P_2^2)^2 + \alpha_{12}(P_1^4 + P_2^4) - \mu_{12}(\varphi_1^2 + \varphi_2^2)\theta_3^2 \\
& + \beta_1(\varphi_1^2 + \varphi_2^2) + \beta_{11}(\varphi_1^2 + \varphi_2^2)^2 + \beta_{12}(\varphi_1^4 + \varphi_2^4) - \kappa_{12}(P_1^2 + P_2^2)\theta_3^2 \\
& + \gamma_1\theta_3^2 + (\gamma_{11} + \gamma_{12})\theta_3^4 - t_{11}(P_1^2\varphi_1^2 + P_2^2\varphi_2^2) - t_{12}(P_1^2\varphi_2^2 + P_2^2\varphi_1^2) \\
& - t_{44}P_1P_2\varphi_1\varphi_2 - (G_{12}\sigma_{22} + G_{11}\sigma_{33})\theta_3^2 \\
& - [Q_{12}\sigma_{22}P_1^2 + Q_{11}\sigma_{22}P_2^2 + Q_{12}\sigma_{33}(P_1^2 + P_2^2)] \\
& - [R_{12}\sigma_{22}\varphi_1^2 + R_{11}\sigma_{22}\varphi_2^2 + R_{12}\sigma_{33}(\varphi_1^2 + \varphi_2^2)] \\
& + \frac{1}{2}\xi_{11}P_{1,1}^2 + \frac{1}{2}\xi_{44}P_{2,1}^2 + \frac{1}{2}v_{11}\varphi_{1,1}^2 + \frac{1}{2}v_{44}\varphi_{2,1}^2 + \frac{1}{2}\omega_{44}\theta_{3,1}^2 \\
& + \frac{1}{2}s_{11}(\sigma_{22}^2 + \sigma_{33}^2) + s_{12}\sigma_{22}\sigma_{33}
\end{aligned} \tag{3}$$

where the two non-zero stress components are given by

$$\sigma_{22} = \frac{U_2 s_{11} - U_3 s_{12}}{s_{11}^2 - s_{12}^2}, \quad \sigma_{33} = \frac{U_3 s_{11} - U_2 s_{12}}{s_{11}^2 - s_{12}^2} \quad (4)$$

with $U_2 = R_{12} [(\varphi_1^e)^2 - \varphi_1^2] - Q_{12} P_1^2 - Q_{11} P_2^2$ and $U_3 = R_{12} [(\varphi_1^e)^2 - \varphi_1^2] - Q_{12} (P_1^2 + P_2^2)$. It should be mentioned that these two stress components are zero inside the domain, while nonzero near the wall. Bulk equilibrium values of the order parameters in the domains are φ_1^e , φ_2^e and θ_3^e . Minimizing the total free energy with respect to polarization P_1 and P_2 , one can easily get

$$2P_1 \left[Q_{12} (\sigma_{22} + \sigma_{33}) + \alpha_1 + \alpha_{11} (P_1^2 + P_2^2) + 2\alpha_{12} P_1^2 - t_{11} \varphi_1^2 - t_{12} \varphi_2^2 - \kappa_{12} \theta_3^2 \right] - \xi_{11} \frac{\partial^2 P_1}{\partial x_1^2} = t_{44} P_2 \varphi_1 \varphi_2 \quad (5a)$$

$$2P_2 \left[Q_{11} \sigma_{22} + Q_{12} \sigma_{33} + \alpha_1 + \alpha_{11} (P_1^2 + P_2^2) + 2\alpha_{12} P_2^2 - t_{11} \varphi_2^2 - t_{12} \varphi_1^2 - \kappa_{12} \theta_3^2 \right] - \xi_{44} \frac{\partial^2 P_2}{\partial x_1^2} = t_{44} P_1 \varphi_1 \varphi_2 \quad (5b)$$

Near the domain wall, one can write order parameters in terms of their deviation from bulk value $\varphi_1 = \varphi_1^e + \delta\varphi_1$, $P_1 = \delta P_1$ and $P_2 = \delta P_2$. Assuming all the deviations are at the same order, expanding Eq. (5) to the first order of small deviation leads to

$$\begin{cases} 2\delta P_1 [\alpha_1 - t_{11} (\varphi_1^e)^2 - t_{12} (\varphi_2^e)^2 - \kappa_{12} (\theta_3^e)^2] - \xi_{11} \frac{\partial^2 \delta P_1}{\partial x_1^2} = t_{44} \delta P_2 \varphi_1^e \varphi_2^e \\ 2\delta P_2 [\alpha_1 - t_{11} (\varphi_2^e)^2 - t_{12} (\varphi_1^e)^2 - \kappa_{12} (\theta_3^e)^2] - \xi_{44} \frac{\partial^2 \delta P_2}{\partial x_1^2} = t_{44} \delta P_1 \varphi_1^e \varphi_2^e \end{cases} \quad (6)$$

where stress relation Eq. (4) is used since all the stress components are also small quantities (proportional to $\delta\varphi_1$) near the domain wall. Assuming $\xi_{11} = \xi_{44} = g$ for simplicity, general solution for this coupled linear equation set is

$$\begin{cases} \delta P_1 = 2C_1 \cosh(A_1 x_1) + 2C_2 \sinh(A_2 x_1) \\ \delta P_2 = 2C_1 \cosh(A_1 x_1) - 2C_2 \sinh(A_2 x_1) \end{cases} \quad (7)$$

with constants C_1 and C_2 , $A_1 = \sqrt{\frac{2[\alpha_1 - t_{11}(\varphi_1^e)^2 - t_{12}(\varphi_2^e)^2 - \kappa_{12}(\theta_3^e)^2] - t_{44}\varphi_1^e\varphi_2^e}{g}}$, and

$A_2 = \sqrt{\frac{2[\alpha_1 - t_{11}(\varphi_1^e)^2 - t_{12}(\varphi_2^e)^2 - \kappa_{12}(\theta_3^e)^2] + t_{44}\varphi_1^e\varphi_2^e}{g}}$. To apply this result to the domain structure in

Figure 1, parameters in different domains are labeled with super-script I, II or III. Since structural parameters satisfy $|\varphi_1^e| = |\varphi_2^e|$, $\varphi_1^{eI} = -\varphi_1^{eII}$ and $\varphi_2^{eI} = \varphi_2^{eII}$, we have $A_1^I = A_2^{II}$ and $A_2^I = A_1^{II}$. At the I-side of the I-II domain wall, distance Δ from the bulk, polarization solutions take the form $\delta P_1 = C_1 e^{A_1^I \Delta} + C_2 e^{A_2^I \Delta}$, $\delta P_2 = C_1 e^{A_1^I \Delta} - C_2 e^{A_2^I \Delta}$, at the II-side, they are $\delta P_1 = C_1 e^{A_2^I \Delta} - C_2 e^{A_1^I \Delta}$, $\delta P_2 = C_1 e^{A_2^I \Delta} + C_2 e^{A_1^I \Delta}$. However, no nonzero coefficients C_1 and C_2 can be found to simultaneously satisfy the anti-symmetric profile of δP_1 together with the symmetric profile of δP_2 observed in experiments. Also, without additional coupling terms, free energy (3) can only generate kink-like or breather-like profiles as discussed by Ref⁵ (also shown in Figure 2) but not the AFE-like odd polarization distribution.

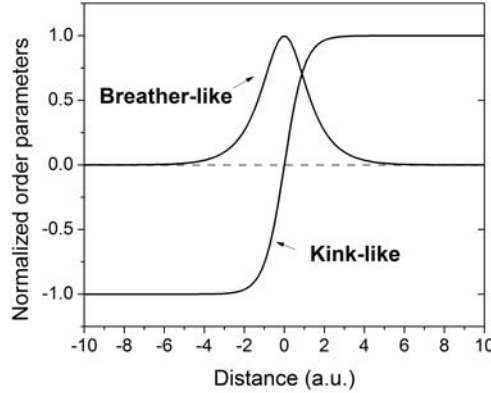


Figure 2. The schematics of the domain wall profiles for the biquadratic coupling. The profile can be either kink-like or breather-like.

We then perform the phase-field simulation by including the effect of flexoelectric coupling. All the simulation settings remain unchanged except that the flexoelectric contribution is added to free energy (2). The contribution of flexoelectricity to the total free energy density can be expressed as

$$f_{flexoelectric} = \frac{1}{2} f_{ijkl} \left(\frac{\partial P_k}{\partial x_j} \varepsilon_{ij} - \frac{\partial \varepsilon_{ij}}{\partial x_k} P_k \right) \quad (8)$$

where f_{ijkl} is the flexoelectric coupling coefficient. Due to lack of existing flexoelectric coupling coefficients, we simply pick the typical values⁴⁹ for ferroelectric perovskites, i.e. $f_{11} = f_{12} = -10$ C/m and $f_{44} = 0$. The gradient energy coefficients of polarization is renormalized accordingly due to the incorporation of the flexoelectricity⁵⁰. The profiles of order parameters obtained from the simulation are plotted in Figure 3. The calculated equilibrium values for the structural order parameters are the same as the previous simulation. In addition, both walls show AFE-like P_1 component at the wall and a ferroelectric P_2 component, which agrees with the previous numerical calculation based on LGD theory⁴. The wall of polarization is around four pseudocubic unit cell thick, which is wider than the wall of octahedra tilts. Comparing Figure 3 (a) and (b), it is found that the P_1 component is invariant with the domain wall structure, while the sign of P_2 is locked with the domain wall angle. This feature can be explained by $P_1 \propto \partial(\phi_1^2)/\partial x_1$ and $P_2 \propto \partial(\phi_1\phi_2)/\partial x_1$ ³⁷. All the above mentioned characteristics of polar domain walls agree qualitatively well with both previous atomistic calculations^{12,14} and experimental observations¹¹, although the agreement is not quantitative due to the lack of flexoelectric coupling coefficients and the gradient energy coefficients. Thus, the flexoelectric coupling can be regarded as, at least, a likely origin of the induced interfacial polar order.

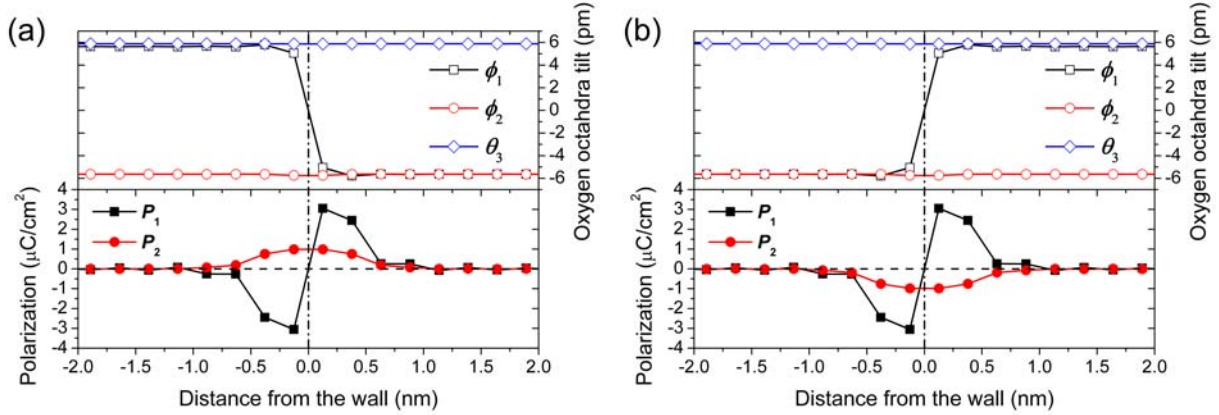


Figure 3. The calculated domain wall profiles from phase-field simulation with flexoelectric contribution. (a) and (b) correspond to the left and right wall in Figure 1. The P_1 component shows an AFE-like profile which is identical in two walls, while the P_2 component changes sign. The profiles of oxygen octahedra tilt are identical to the phase-field simulation results without including flexoelectric effect.

To better understand the effect of flexoelectric coupling, we carry out an analysis similar to the biquadratic case [Eq. (3) to Eq. (6)]. With the flexoelectric coupling term, an additional term

$$f_{flexoelectric}^B = \frac{1}{2} F_{12} \left[\frac{\partial P_1}{\partial x_1} (\sigma_{22} + \sigma_{33}) - \frac{\partial (\sigma_{22} + \sigma_{33})}{\partial x_1} P_1 \right] \quad (9)$$

is added to Eq. (3). Here $F_{ij} = s_{ik} f_{kj}$, with i, j , and k running from 1 to 3. Expressions for the two non-zero stress components in Eq. (4) still holds with $U_2 = R_{12} [(\varphi_1^e)^2 - \varphi_1^2] - Q_{12} P_1^2 - Q_{11} P_2^2 + F_{12} \frac{\partial P_1}{\partial x_1}$ and

$U_3 = R_{12} [(\varphi_1^e)^2 - \varphi_1^2] - Q_{12} (P_1^2 + P_2^2) + F_{12} \frac{\partial P_1}{\partial x_1}$. Minimizing the total energy with respect to P_1 gives an

equation similar to Eq. (5a) with an additional term $-F_{12} \frac{\partial (\sigma_{22} + \sigma_{33})}{\partial x_1}$ on the left hand side, while the

same result Eq. (5b) is reached for P_2 . From here, we take a different approach in analyzing the solution by looking at the linear order expansion of small deviations δP_1 and δP_2 at both sides of the domain wall.

For the configuration demonstrated in Figure 3, the linear order equation is a good approximation at both sides of the wall as long as δP is small (for example at $\pm 0.75nm$). For δP_1 , equations are

$$\begin{cases} 2A\delta P_1^+ - \xi_{11} \frac{\partial^2 \delta P_1^+}{\partial x_1^2} = F_{12} \frac{\partial (\sigma_{22}^+ + \sigma_{33}^+)}{\partial x_1} & (10a) \\ 2A\delta P_1^- - \xi_{11} \frac{\partial^2 \delta P_1^-}{\partial x_1^2} = F_{12} \frac{\partial (\sigma_{22}^- + \sigma_{33}^-)}{\partial x_1} & (10b) \end{cases}$$

with superscript "+" and "-" for different side of the wall, and $A = \alpha_1 - t_{11}(\varphi_1^e)^2 - t_{12}(\varphi_2^e)^2 - \kappa_{12}(\theta_3^e)^2$. To focus on the effect of flexoelectric coupling, we ignore the biquadratic coupling in deriving Eq. (10) (i.e. $t_{44} = 0$). In this case, polarization δP_1^\pm is determined by the changing rate of stress along x_1 . A similar equation for $\delta \varphi_1$ can be written as

$$\begin{cases} 2\tilde{A}\delta \varphi_1^+ - v_{11} \frac{\partial^2 \delta \varphi_1^+}{\partial x_1^2} + R_{12} (\sigma_{22}^+ + \sigma_{33}^+) = 0 \\ -2\tilde{A}\delta \varphi_1^- + v_{11} \frac{\partial^2 \delta \varphi_1^-}{\partial x_1^2} - R_{12} (\sigma_{22}^- + \sigma_{33}^-) = 0 \end{cases} \quad (11)$$

with $\delta\varphi_1$ measures the deviation from bulk value (i.e. $\varphi_1 = -\varphi_1^e + \delta\varphi_1^+$ at the "+" side and $\varphi_1 = \varphi_1^e - \delta\varphi_1^-$ at the "-" side for the setup in Figure 3a) and $\tilde{A} = \beta_1 + \beta_{11}(\varphi_2^e)^2 + 3(\varphi_1^e)^2(\beta_{11} + 2\beta_{12}) - \mu_{12}(\theta_3^e)^2$. Since φ_1 is a known even function, Eq. (11) should give $\delta\varphi_1^+ = \delta\varphi_1^-$ which requires the stress term satisfies $\sigma_{22}^+ + \sigma_{33}^+ = \sigma_{22}^- + \sigma_{33}^-$. Back to Eq. (10), the right-hand-sides of Eq. (10a) and (10b) have opposite signs because the derivative of an even stress function is an odd function. This indicates that the polarization given by Eq. (10) should satisfy $\delta P_1^+ = -\delta P_1^-$ i.e. an odd polarization profile. These simple observations on the asymptotic polarization behavior near the bulk provides an insight into the effect of flexoelectric coupling and attributes the commonly observed odd polarization profile (or AFE-like) across the domain wall directly to the stress variation and flexoelectric coupling in the system.

As discussed in Ref. ¹⁰, the major difference in flexoelectric coupling and the biquadratic coupling is whether the stress or the stress gradient at the domain wall dominates. As shown above, the width of a domain wall is on the magnitude of nanometers, which give rise to a strain gradient on the magnitude of 10^7 m^{-1} . Such a huge strain gradient makes the flexoelectric effect dominant. For example, it is demonstrated that the additional polarization component to the conventional-believed Ising-like 180° ferroelectric domain walls are driven by the flexoelectric effect^{6,39}.

Another possible explanation for the origin of polar domain walls is the so-called improper AFD-AFE coupling¹², which is demonstrated universal in perovskite with AFD ⁵¹. The coupled AFE modes include X_5^+ mode (Ca and O atoms at Wyckoff 4c moving along $[110]$) and R_5^+ mode (Ca atoms moving along $[\bar{1}10]$). To consider the AFD-AFE coupling in CaTiO_3 , the total free energy needs to include $X_1\varphi_1\theta_3$, $X_2\varphi_2\theta_3$, $R_1\varphi_1\theta_3^2$, $R_2\varphi_2\theta_3^2$ ⁵¹, and some more terms by symmetry⁵². The total free energy with the two AFE modes (X_5^+ and R_5^+) can be written as^{12,52,53}

$$\begin{aligned}
f^T(X_1, X_2, R_1, R_2, \varphi_1, \varphi_2, \theta_3) = & \nu_1(X_1^2 + X_2^2) + \nu_{11}(X_1^2 + X_2^2)^2 + \nu_{12}(X_1^4 + X_2^4) \\
& + \tau_1(R_1^2 + R_2^2) + \tau_{11}(R_1^2 + R_2^2)^2 + \tau_{12}(R_1^4 + R_2^4) \\
& + \beta_1(\varphi_1^2 + \varphi_2^2) + \beta'_{11}(\varphi_1^2 + \varphi_2^2)^2 + \beta'_{12}(\varphi_1^4 + \varphi_2^4) \\
& + \gamma_1\theta_3^2 + (\gamma'_{11} + \gamma'_{12})\theta_3^4 - \mu'_{12}(\varphi_1^2 + \varphi_2^2)\theta_3^2 \\
& + \overline{\omega}_X(X_1\varphi_1 + X_2\varphi_2)\theta_3 + \overline{\omega}_R(R_1\varphi_1\varphi_2^2 + R_2\varphi_2\varphi_1^2) \\
& + \overline{\omega}_\theta(R_1\varphi_1\theta_3^2 + R_2\varphi_2\theta_3^2) + \vartheta_{11}(X_1^2 + X_2^2)(R_1^2 + R_2^2) \quad (8) \\
& + n_{11}(\varphi_1^2 + \varphi_2^2)(X_1^2 + X_2^2) + \bar{n}_{12}(X_1^2 + X_2^2)\theta_3^2 \\
& + m_{11}(\varphi_1^2 + \varphi_2^2)(R_1^2 + R_2^2) + \bar{m}_{12}(R_1^2 + R_2^2)\theta_3^2 \\
& + \frac{1}{2}\zeta_{11}X_{1,1}^2 + \frac{1}{2}\zeta_{44}X_{2,1}^2 + \frac{1}{2}\xi_{11}R_{1,1}^2 + \frac{1}{2}\xi_{44}R_{2,1}^2 \\
& + \frac{1}{2}v_{11}\varphi_{1,1}^2 + \frac{1}{2}v_{44}\varphi_{2,1}^2 + \frac{1}{2}\omega_{44}\theta_{3,1}^2
\end{aligned}$$

Since the coefficients of AFD-AFE coupling are not available, we cannot perform numerical simulations. But by a similar asymptotic analysis as we did for biquadratic coupling, we find that the signs of X_1 and R_1 are locked with φ_1^e . It simply suggests that the AFE-AFD coupling may capture the polar domain wall features. However, this hypothesis cannot explain the similar AFE-like polarizations at the 180° domain walls of AFD-free tetragonal BaTiO_3 ^{6,39} or PbTiO_3 ^{29,54}, which can be well resolved by the flexoelectric effect. The essential difference between the flexoelectric coupling and the improper AFD-AFE coupling is that the former describes the interaction between the optical mode (polarization) and the acoustic mode (AFD); while the latter describes the competition between two acoustic modes (AFE and AFD). As demonstrated by first-principles calculations⁵⁵, the optical mode is inherently unstable in CaTiO_3 . Simply by manipulating the epitaxial strain, the AFD can be suppressed and thus give rise to polarization^{42,55}. Therefore, it is reasonable to conclude that the emergence of AFE-like polarization at the domain wall is due to the inherent instability of the optical mode. But more experimental and theoretical studies are needed to further clarify the mechanism.

To summarize, employing the phase-field modeling and asymptotic analysis we investigated the origin of the polar domain walls in incipient ferroelectrics CaTiO_3 by including several coupling terms in the GLD theory. It is shown that the biquadratic coupling of AFD and polarization alone is unable to produce all the key features of the polarization at the domain walls, while the domain wall structures generated by flexoelectric coupling agree qualitatively with both previous calculations and experimental observations. The improper AFD-AFE coupling may also give rise to the complex polarization distribution at the domain wall, but it ignores the instability of the optical mode (polarization) and cannot explain the similar

polarization profiles of the pure ferroelectric domain walls. However, further studies are still needed to exclude this possibility.

Acknowledgement

This work was supported by the NSF through grants DMR-1410714, DMR-1210588 and DMR 1234096. The computer simulations were carried out on the LION and Cyberstar clusters at the Pennsylvania State University, in part supported by instrumentation (Cyberstar Linux cluster) funded by the NSF through Grant OCI-0821527.

References

- ¹ D. Meier, J. Seidel, A. Cano, K. Delaney, Y. Kumagai, M. Mostovoy, N.A. Spaldin, R. Ramesh, and M. Fiebig, *Nat. Mater.* **11**, 1 (2012).
- ² J. Seidel, L.W. Martin, Q. He, Q. Zhan, A. Rother, M.E. Hawkridge, P. Maksymovych, P. Yu, M. Gajek, N. Balke, S. V Kalinin, S. Gemming, F. Wang, G. Catalan, J.F. Scott, N.A. Spaldin, J. Orenstein, R. Ramesh, and Y.H. Chu, *Nat. Mater.* **8**, 229 (2009).
- ³ E.A. Eliseev, A.N. Morozovska, G.S. Svechnikov, P. Maksymovych, and S. V Kalinin, *Phys. Rev. B* **85**, 045312 (2012).
- ⁴ E.A. Eliseev, A.N. Morozovska, Y. Gu, A.Y. Borisevich, L.-Q. Chen, V. Gopalan, and S. V Kalinin, *Phys. Rev. B* **86**, 085416 (2012).
- ⁵ B. Houchmandzadeh, J. Lajzerowicz, and E.K.H. Salje, *J. Phys. Condens. Matter* **3**, 5163 (1991).
- ⁶ P. V Yudin, A.K. Tagantsev, E.A. Eliseev, A.N. Morozovska, and N. Setter, *Phys. Rev. B* **86**, 134102 (2012).
- ⁷ M. Calleja, M.T. Dove, and E.K.H. Salje, *J. Phys. Condens. Matter* **15**, 2301 (2003).
- ⁸ L. Goncalves-Ferreira, S.A.T. Redfern, E. Artacho, E.K.H. Salje, and W.T. Lee, *Phys. Rev. B* **81**, 24109 (2010).
- ⁹ J.F. Scott, E.K.H. Salje, and M.A. Carpenter, *Phys. Rev. Lett.* **109**, 187601 (2012).
- ¹⁰ E.K.H. Salje, O. Aktas, M.A. Carpenter, V. V Laguta, and J.F. Scott, *Phys. Rev. Lett.* **111**, 247603 (2013).
- ¹¹ S. Van Aert, S. Turner, R. Delville, D. Schryvers, G. Van Tendeloo, and E.K.H. Salje, *Adv. Mater.* **24**, 523 (2012).
- ¹² P. Barone, D. Di Sante, and S. Picozzi, *Phys. Rev. B* **89**, 144104 (2014).

- ¹³ H. Yokota, H. Usami, R. Haumont, P. Hicher, J. Kaneshiro, E.K.H. Salje, and Y. Uesu, *Phys. Rev. B* **89**, 144109 (2014).
- ¹⁴ L. Goncalves-Ferreira, S.A.T. Redfern, E. Artacho, and E.K.H. Salje, *Phys. Rev. Lett.* **101**, 097602 (2008).
- ¹⁵ G. Catalan, J. Seidel, R. Ramesh, and J.F. Scott, *Rev. Mod. Phys.* **84**, 119 (2012).
- ¹⁶ A. Aird and E.K.H. Salje, *J. Phys. Condens. Matter* **10**, L377 (1998).
- ¹⁷ J. Guyonnet, I. Gaponenko, S. Gariglio, and P. Paruch, *Adv. Mater.* **23**, 5377 (2011).
- ¹⁸ W.J. Merz, *Phys. Rev.* **95**, (1954).
- ¹⁹ S.S.P. Parkin, M. Hayashi, and L. Thomas, *Science (80-.)*. **320**, 190 (2008).
- ²⁰ T. Sluka, A.K. Tagantsev, P. Bednyakov, and N. Setter, *Nat. Commun.* **4**, 1 (2013).
- ²¹ R. Xu, J. Karthik, A.R. Damodaran, and L.W. Martin, *Nat. Commun.* **5**, 3120 (2014).
- ²² X.-K. Wei, A.K. Tagantsev, A. Kvasov, K. Roleder, C.-L. Jia, and N. Setter, *Nat. Commun.* **5**, 3031 (2014).
- ²³ R.K. Vasudevan, W. Wu, J.R. Guest, A.P. Baddorf, A.N. Morozovska, E.A. Eliseev, N. Balke, V. Nagarajan, P. Maksymovych, and S. V Kalinin, *Adv. Funct. Mater.* 2592 (2013).
- ²⁴ Q. Zhang and W. a. Goddard, *Appl. Phys. Lett.* **89**, 182903 (2006).
- ²⁵ Y.-H. Shin, I. Grinberg, I.-W. Chen, and A.M. Rappe, *Nature* **449**, 881 (2007).
- ²⁶ M. Taherinejad, D. Vanderbilt, P. Marton, V. Stepkova, and J. Hlinka, *Phys. Rev. B* **86**, 155138 (2012).
- ²⁷ J.C. Wojdeł and J. Íñiguez, *Phys. Rev. Lett.* **112**, 247603 (2014).
- ²⁸ E.A. Eliseev, P. V Yudin, S. V Kalinin, N. Setter, A.K. Tagantsev, and A.N. Morozovska, *Phys. Rev. B* **87**, 054111 (2013).
- ²⁹ D. Lee, R.K. Behera, P. Wu, H. Xu, Y.L. Li, S.B. Sinnott, S.R. Phillpot, L.Q. Chen, and V. Gopalan, *Phys. Rev. B* **80**, 060102(R) (2009).
- ³⁰ B. Meyer and D. Vanderbilt, *Phys. Rev. B* **65**, 104111 (2002).
- ³¹ A.N. Morozovska, R.K. Vasudevan, P. Maksymovych, S. V Kalinin, and E.A. Eliseev, *Phys. Rev. B* **86**, 085315 (2012).
- ³² J. Padilla, W. Zhong, and D. Vanderbilt, *Phys. Rev. B* **53**, 5969 (1996).
- ³³ D.A. Scrymgeour, V. Gopalan, A. Itagi, A. Saxena, and P.J. Swart, *Phys. Rev. B* **71**, 184110 (2005).

- ³⁴ Y. Wang, C. Nelson, A. Melville, B. Winchester, S. Shang, Z. Liu, D.G. Schlom, X. Pan, and L. Chen, *Phys. Rev. Lett.* **110**, 267601 (2013).
- ³⁵ M.E. Lines and A.M. Glass, *Principles and Applications of Ferroelectrics and Related Materials* (Oxford University Press, Oxford, 1977).
- ³⁶ F. Jona and G. Shirane, *Ferroelectric Crystals*, Dover (DOVER PUBLICATIONS INC. Mineola, New York, 1993).
- ³⁷ A.N. Morozovska, E.A. Eliseev, M.D. Glinchuk, L.-Q. Chen, and V. Gopalan, *Phys. Rev. B* **85**, 094107 (2012).
- ³⁸ A.N. Morozovska, E.A. Eliseev, S. V Kalinin, L.-Q. Chen, and V. Gopalan, *Appl. Phys. Lett.* **100**, 142902 (2012).
- ³⁹ Y. Gu, M. Li, A.N. Morozovska, Y. Wang, E.A. Eliseev, V. Gopalan, and L.-Q. Chen, *Phys. Rev. B* **89**, 174111 (2014).
- ⁴⁰ A.P. Levanyuk and D.G. Sannikov, *Sov. Phys. Uspekhi* **17**, 199 (1974).
- ⁴¹ R. Ahluwalia, A.K. Tagantsev, P. Yudin, N. Setter, N. Ng, and D.J. Srolovitz, *Phys. Rev. B* **89**, 174105 (2014).
- ⁴² Y. Gu, K. Rabe, E. Bousquet, V. Gopalan, and L.-Q. Chen, *Phys. Rev. B* **85**, 064117 (2012).
- ⁴³ L.-Q. Chen, *Annu. Rev. Mater. Res.* **32**, 113 (2002).
- ⁴⁴ A.G. Khachaturyan, *Theory of Structural Transformations in Solids* (DOVER PUBLICATIONS INC., Mineola, New York, 2008), p. 576.
- ⁴⁵ Y.L. Li, S.Y. Hu, Z.K. Liu, and L.Q. Chen, *Appl. Phys. Lett.* **81**, 427 (2002).
- ⁴⁶ M. Yashima and R. Ali, *Solid State Ionics* **180**, 120 (2009).
- ⁴⁷ B.J. Kennedy, C.J. Howard, and B.C. Chakoumakos, *J. Phys. Condens. Matter* **11**, 1479 (1999).
- ⁴⁸ N. Wang, R. Spatschek, and a. Karma, *Phys. Rev. E* **81**, 051601 (2010).
- ⁴⁹ J. Hong and D. Vanderbilt, *Phys. Rev. B* **88**, 174107 (2013).
- ⁵⁰ A.K. Tagantsev, E. Courtens, and L. Arzel, *Phys. Rev. B* **64**, 224107 (2001).
- ⁵¹ L. Bellaiche and J. Íñiguez, *Phys. Rev. B* **88**, 014104 (2013).
- ⁵² H.T. Stokes and D.M. Hatch, Stokes.byu.edu/isotropy.html (n.d.).
- ⁵³ C.-J. Eklund, *Interplay of Strain, Polarization, and Magnetic Ordering in Complex Oxides from First Principles*, Rutgers University, 2010.

⁵⁴ R.K. Behera, C. Lee, D. Lee, A.N. Morozovska, S.B. Sinnott, A. Asthagiri, V. Gopalan, and S.R. Phillpot, *J. Phys. Condens. Matter* **23**, 175902 (2011).

⁵⁵ C.-J. Eklund, C.J. Fennie, and K.M. Rabe, *Phys. Rev. B* **79**, 220101(R) (2009).